ChemComm

Accepted Manuscript

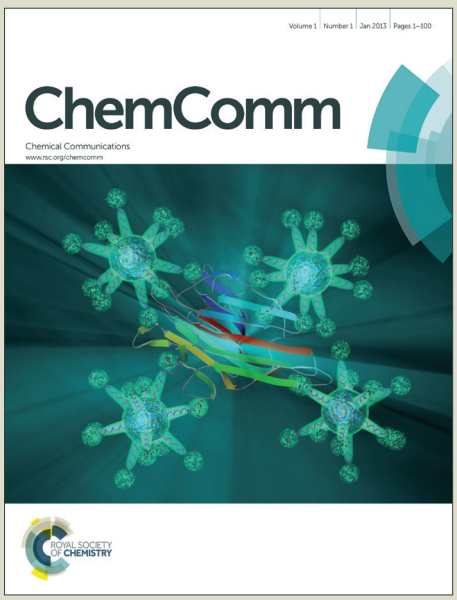

ROYAL SOCIETY OF CHEMISTRY

www.rsc.org/chemcomm

Table of content

Sodium dendrites and side reactions were investigated in the sodium oxygen batteries, of which the cyclability was greatly improved by a sodium ion selective polymer membrane.

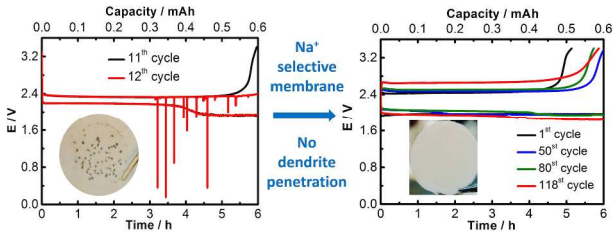

Cite this: DOI: 10.1039/c0xx00000x

www.rsc.org/xxxxxx

ARTICLE TYPE

Investigating dendrites and side reactions in sodium oxygen batteries for improved cycle lives

Xuanxuan Bi,[a] Xiaodi Ren,[a] Zhongjie Huang,[a] Mingzhe Yu,[a] Eric Kreidler[b] and Yiying Wu*[a]

Received (in XXX, XXX) Xth XXXXXXXXX 20XX, Accepted Xth XXXXXXXXX 20XX

DOI: 10.1039/b000000x

The development of sodium-oxygen batteries with high round-trip efficiencies is hindered by the short cycle lives. Sodium dendrite formation and oxygen crossover are identified as two major issues. By employing an ion selective membrane, the cycle life of sodium oxygen batteries has been greatly improved.

Due to high theoretical gravimetric energy densities, metal-air (-oxygen) batteries have attracted extensive interests for potential applications in transportation, portable electronics, and stationary energy storage systems[1]. However, lithium-oxygen ($Li-O_2$) batteries undergo large polarizations (> 1 V) during the charging process in the absence of electrocatalysts, leading to poor round-trip efficiencies[2]. Hartmann et al. reported that a much lower charge overpotential of 200 mV was obtained by sodium oxygen ($Na-O_2$) batteries with ether based electrolyte, which made them a promising competitor in metal-oxygen battery chemistries[3]. Compared to the multi-step reaction in $Li-O_2$ batteries, $Na-O_2$ batteries undergo a single-electron transfer reaction:

$$Na + O_2 \leftrightarrow NaO_2 \quad (E^0 = 2.27\ V),$$

where sodium superoxide (NaO_2) is characterized as the discharge product. Almost the same time, a one-electron potassium ($K-O_2$) battery based on potassium superoxide was also demonstrated in our group with a charge/discharge voltage hysteresis as small as 50 mV[4].

Despite the promising cyclability gained from the lower charging potential, the development of $Na-O_2$ batteries was greatly hindered by the poor cycle life which was ascribed to dendrite formation, instability of electrolytes and by-product formation[5-8]. Inspired by the complex by-product formation reactions at the cathode side of $Li-O_2$ batteries[5], most of the researches have been focused on the characterization of cathodes, e.g., by-products and the effects of cathode morphology to the cyclability performance in $Na-O_2$ batteries. Hartmann and Bender et al. observed that the conducting salt decomposed to sodium fluoride and sodium sulfite on the carbon fiber cathode in $Na-O_2$ batteries.[6] Zhao et al. detected sodium hydroxide and sodium carbonate as decomposition products on vertically aligned carbon nanotubes.[7] However, McCloskey et al. pointed out that the cleaner cathode reactions in $Na-O_2$ compared to $Li-O_2$ were less concerned and the low cycle life was perhaps caused by the Na anode.[8] The possible contribution to the cyclability from the Na anode has rarely been reported in Na batteries.[9] It is well known that the lithium dendrite is a safety concern in lithium ion batteries. However, with complicated effects from an oxygen rich environment, there has been no report on the dendrite formation in $Li-O_2$ and $K-O_2$ batteries.[2(a),4] Hartmann et al. observed dendrite growing into the polymer separator, which had detrimental effect to the $Na-O_2$ battery. By replacing the polymer separator with a solid-state electrolyte (sodium-beta-alumina) dendrite penetration was suppressed; however, the battery performance was not shown in their work and the effect of dendrite formation was not clearly understood.[6(a)] On the other hand, the reaction of metal anode with electrolyte was not fully investigated. Although a stable solid electrolyte interfaces (SEI) layer could be formed on the surface of Li-ion battery anode, it was recently reported that in $Li-O_2$ batteries, more complicated reactions could occur on the Li anode in the presence of O_2 crossed from the air cathode.[10] Our group also prove that oxygen crossover significantly limits the low cycle life of $K-O_2$ batteries.[11]

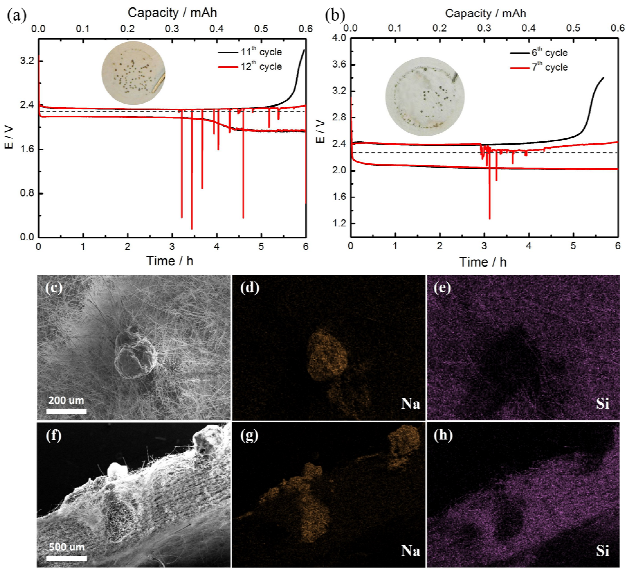

Figure 1. Discharge/charge profiles of a $Na-O_2$ battery for the last two cycles in (a) DME and (b) diglyme. The inserts are the images of the glass fiber separator facing to the Na electrode. Dashed lines are the standard potentials. SEM and EDS mapping images of (c-e) the top-view and (f-h) cross-section of Na dendrite in GF separators.

Here we show that dendrite formation in $Na-O_2$ batteries is the

primary reason for the failure of batteries while the reaction of Na anode with electrolyte with the presence of O_2 plays a vital role in the cycling performance decline. To address the dendrite issue, the first use of a sodium ion selective polymer membrane[12,13] incorporated as part of a separator in a Na-O_2 battery is reported in this work. Using 0.16 mA cm^{-2} geometric current density, cycling lives of 110 cycles in 1,2-dimethoxyethane (DME) and 90 cycles in diglycol methyl ether (diglyme) were achieved. Additionally, the by-products were investigated in both electrodes. Since the Nafion-Na^+ membrane selectively block the diffusion of anions through the batteries, it helped distinguish the anode side reactions from the cathode ones, which proved that the decomposition occurred mostly in the Na anode instead of the cathode. These results highlight the significance of solving anode issues in sodium oxygen batteries and potentially pave the way for further improving the performance and cyclability of the battery chemistries.

The Na-O_2 batteries were constructed as described in the experimental (Supplementary Information). Glass fibers (GF) were used as the separator. To minimize the interference from the cathode (namely oxygen diffusion, electrolyte decomposition, and pore blocking), ether solvents and discharge conditions were carefully addressed. DME was selected as the solvent utilized in the 0.5 M sodium trifluoromethanesulfonate ($NaCF_3SO_3$, sodium triflate) electrolyte due to higher reported oxygen solubility and oxygen diffusion coefficients[14]. 0.5 M Na triflate in diglyme was used as a comparison. These characteristics improve the oxygen diffusion in the air electrode and facilitate the formation of sodium superoxide.

Based on battery performance tests, the cycle lives of Na-O_2 batteries using DME and diglyme based electrolytes fluctuate between 6 cycles to 12 cycles. The discrepancy is likely due to the variations of dendrite formation rates on the varying Na surfaces in each cell or mechanical compressions. The discharge/charge profiles of 11^{th} and 12^{th} cycles in DME based electrolyte are shown in Figure 1a. For the 11^{th} cycle, the discharging voltage of 2.2 V and a charging voltage of 2.4 V are displayed. The small voltage gap implies the reversible reaction process, $Na + O_2 \leftrightarrow NaO_2$. X-ray diffraction confirms the only product, NaO_2, shown in Figure S1. In diglyme (Figure 1b), the same scenario is observed in the 6^{th} cycle. However, voltage fluctuations during the charging process occurred after the 11^{th} cycle in DME and the 6^{th} cycle in diglyme. After disassembling the failed batteries, a number of spots were observed at the surface of GF facing the metal anode (inserts in Figure 1a). It indicates that Na dendrites caused the shorting of the batteries. Upon charge, the uneven deposition of sodium metal induces the formation of dendrites which grow through the GF separator and ultimately contact the cathode. After the short is established, the large current flowing through dendrite would generate heat sufficient to melt the Na dendrite, thus cutting off its contact to the air electrode, which will restore the battery to its previous working potential and result in the voltage fluctuations[15].

To verify the dendrite penetration issue, scanning electron microscope (SEM) and energy dispersive X-ray spectroscopy (EDS) mapping were carried on a GF separator of a Na-O_2 battery with DME based electrolyte after 6 cycles discharge/charge process. Figure 1c shows the top-view SEM image of GF (faced to the air electrode) from which a thin top layer was peeled off in order to catch sight of the tip of Na dendrite. The cross-section SEM image of GF separator is displayed in Figure 1f. The topside of the separator in the image was attaching to the anode and the bottom side was facing to the cathode. As can be seen, the dendrite has grown into the glass fibers and almost reached to the cathode. After 6 cycles, the Na metal grows across more than 80% of the thickness of the separator predicting the short in few cycles. EDS mapping proves the distributions of dendrite (Na element) and GFs (Si element, Na_2SiO_3). The major sodium area in Figure 1d can be assigned to the Na dendrite or the SEI layer on the dendrite. Moreover, the area of sodium at the right bottom stands for the root of the dendrite tip. For the rest of the area, the evenly distributed Na is from the GF. To further prove the dendrite penetration, the GF separator was replaced after the failure of the battery and the following cycles have smooth charging curve (Figure S2). The results clearly prove that Na dendrites grow and penetrate into the GF separator and induce the shorting of the battery.

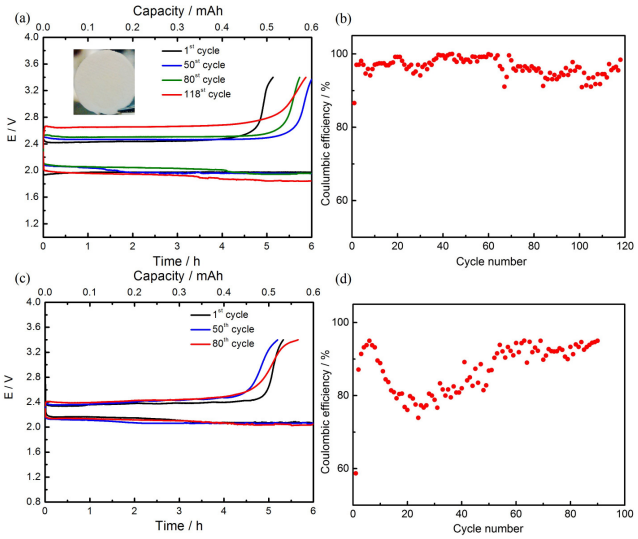

Figure 2. a) Discharge/charge profiles and b) Coulombic efficiency with Nafion-Na^+ membrane in DME. Insert is the glass fiber separator in air electrode facing towards the Nafion-Na^+ membrane. c) Discharge/charge profiles and d) Coulombic efficiency with Nafion-Na^+ membrane in diglyme.

To prevent dendrite penetration, a sodium ion selective membrane was employed between two GF separators in the cell construction. The good mechanical strength of Nafion membranes is postulated to prevent dendrite penetration to the air electrode. Water contents were similar in electrolytes before and after the immersion of Nafion-Na^+ membrane, which proves no water contamination from the membrane (Table S4). The ionic conductivity of the Nafion-Na^+ membrane was calculated to be 2.46e-5 S cm^{-1} at 21 ^oC (see Figure S3 & Table S1). As a comparison, the ionic conductivity of the electrolyte within the GF separator was also tested in this work and the average value is 4.62e-4 S cm^{-1} (Figure S4 & Table S2). The total Ohmic loss from the separator/membrane is approximately 30 mV (Table S3). The voltage profiles with and without Nafion-Na^+ membrane are compared in Figure S5. The slightly differences are consistent with the predicted Ohmic loss from the membrane.

The incorporation of the Nafion-Na^+ membranes greatly

improves the cyclability of Na-O_2 batteries in both DME and diglyme based electrolytes. Discharge/charge profiles of 1st, 50th, 118th cycles in DME are shown in Figure 2a. The discharge/charge voltages are reproducible for the first 80 cycles, after which the charging voltage gradually increased from 2.50 V in the 80th cycle to 2.65 V in the 118th cycle. The expanded voltage gap results from increased polarization most likely due to the accumulation of side products in the air electrode and the growth of a SEI layer on metal surface. Although larger polarization is observed after 80 cycles, Coulombic efficiencies of over 95% were maintained throughout the tests (Figure 2b). The insert in Figure 2a shows the clean surface of the GF from the cathode side facing the Nafion-Na^+ membrane after 118 cycles. As expected, there was no indication of dendrite penetration through the Nafion-Na^+ membrane. Figures 2c and 2d display the voltage profiles and Coulombic efficiency for the cell utilizing diglyme based electrolyte. Good reproducibility and high Coulombic efficiencies prove that the Nafion-Na^+ membrane efficiently prevents dendrite penetration and increases cycling performance of Na-O_2 batteries.

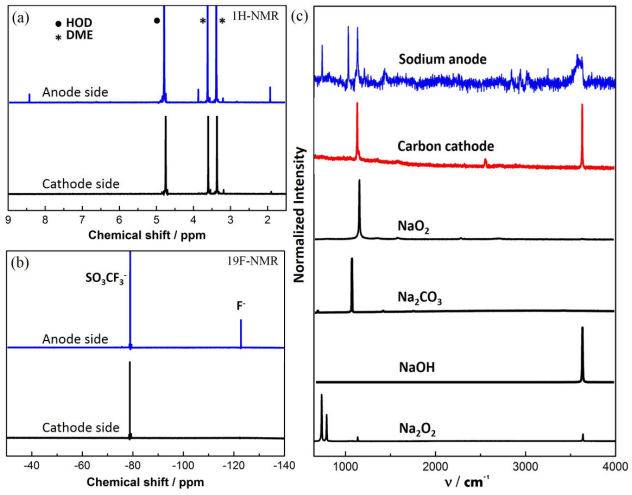

Figure 3. (a) ^{1}H-NMR and (b) ^{19}F-NMR of DME based electrolyte in GF separators from the anode side and the cathode side after 6 cycles. (c) Raman spectra of reference materials and electrodes after 120 cycles. Nafion-Na^+ membranes were used in the cells.

After the failure of the Na-O_2 battery with Nafion-Na^+ in DME (after 120 cycles), the battery was taken apart and no metallic Na was observed in the anode. The leftovers show a light grey color without metallic luster, which indicates the depletion of sodium. To measure the depletion rate of Na, cycling efficiencies of Na in the anode was calculated and the cycling efficiency for each cycle ranged from 60%-80%, as shown in Figure S6. In order to get more insight to the underlying causes, the side products were investigated in both anode and cathode. With Nafion-Na^+ membrane as a part of separator, anions diffusion between the two electrodes has been blocked, giving us the opportunity to explore the decomposition of the electrolyte separately. 0.5 M sodium triflate in DME was used as electrolyte. After 6 cycles, the GF separators from both sides were peeled off from the Nafion-Na^+ membrane and then immersed in D_2O, respectively for NMR measurement. ^{1}H-NMR spectra of the electrolyte from the anode are shown in Figure 3a. The peaks at 8.5 ppm and 1.9 ppm are assigned to formate ($HCOO^-$) and acetate (CH_3COO^-) respectively.[16] At 3.8 ppm, the signal is assigned to methoxyactate ($CH_3OCH_2COO^-$).[11] The small peak at 3.2 ppm is from the conducting salt, sodium triflate.[17] Interestingly, compared to the anodic electrolyte, the cathodic electrolyte only shows a small peak of CH_3COO^-. This is consistent with the argument that the cathode experiences less decomposition than in Li-O_2.[8] From ^{19}F-NMR, as shown in Figure 3b, the peak at -79 ppm is the characteristic peak of triflate species ($SO_3CF_3^-$) and the peak at -122 ppm is from fluoride species (F^-).[18]

The missing peak at -122 ppm in the cathode side indicates the Na triflate is barely decomposed in the cathode. The results indicate both DME solvent and Na triflate were decomposed in the Na anode. Since all the by-products detected to be oxidative compounds, it can be explained that oxygen crossover induces the decomposition of electrolyte with the presence of Na.

The light grey colored solids in the anode were detected by Raman spectroscopy. Figure 3c shows the Raman spectra of both electrodes and the standard peaks of reference materials. From the sodium anode, the peaks at 1080 cm^{-1}, 1156 cm^{-1} and 3638 cm^{-1} are from sodium carbonate (Na_2CO_3), sodium superoxide (NaO_2) and sodium hydroxide (NaOH), respectively. The peak located at 750 cm^{-1} is most likely from sodium peroxide (Na_2O_2). Other small peaks cannot be clearly identified but they suggest the complex products on sodium surface. The formation of NaO_2 and Na_2O_2 is originated from the reaction between Na and the oxygen solvated in the electrolyte. Na_2CO_3 and NaOH are related to the decomposition of the electrolyte with the presence of oxygen. For the carbon cathode, only the signals of NaO_2 and NaOH were detected. NaOH may originate from the decomposition of electrolyte or from possible moisture contamination. The remnant peak of NaO_2 shows that not all NaO_2 was accessible during charge, which is consistent with the previous report[6(a)]. The built-up sodium superoxide would lead to low apparent Coulombic efficiency and passivation of the cathode surface.

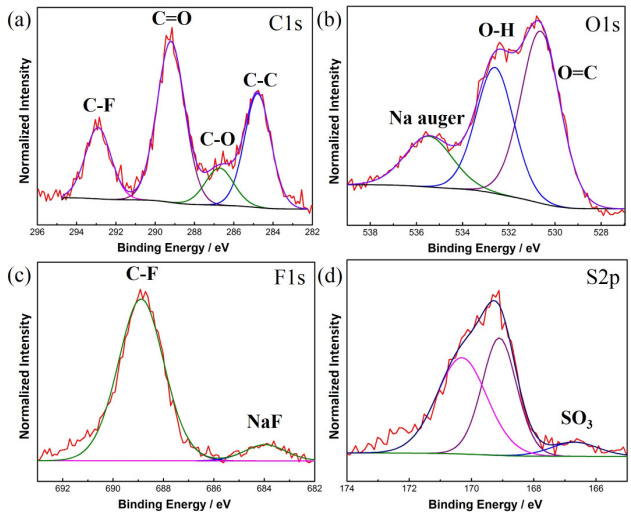

Figure 4. (a) C1s, (b) O1s, (c) F1s and (d) S2p XPS spectra of the Na anode after 120 cycles in a cell with Nafion-Na^+ membrane.

To understand the decomposition products in the SEI layer, C1s, O1s, F1s and S2p spectra on the Na anode were obtained in

XPS, as shown in Figure 4. All spectra were calibrated by the standard position of C-C bond at 284.8 eV. In C1s spectrum, the peaks at 286.7 eV and 292.9 eV are assigned to C-O bond from DME and C-F bond (-CF_3 group) from Na triflate. The large peak at 289.2 eV is most likely from carbonate groups[6,18]. O1s spectra show the signals of Na_2CO_3 and NaOH 531.5 eV at 532.8 eV, showing the decomposition of DME solvent. In F1s spectra, peaks at 683.9 eV and 688.9 eV are from fluoride species (NaF) and triflate (C-F), respectively. The peak located at 166.7 eV in S2p spectra is from the sulfite species. The peaks of fluoride and sulfite indicate the decomposition of sodium salt, Na triflate, in the anode.

A proposed electrolyte decomposition mechanism was reported recently by our group in K-O_2 batteries.[11] Given the similar products detected in the anode, the decomposition mechanism of DME solvent can be applied in Na-O_2 batteries. The solvated electrons generated from the alkali metal react with DME solvent to form DME anion. It further reacts with oxygen and goes through the C-O bond cleavage to form different oxidative products. The investigation of side products in both electrodes implies that the Na anode brought up more issues than the carbon cathode. In addition, different from K-O_2 batteries, the side products formed in the Na SEI layer are ion conductive and the accumulation of side products cannot cause the failure of the battery only if the sodium is fully depleted. Hence, metal protection and oxygen crossover prevention are critical for improving the cyclability of Na-O_2 batteries.

Conclusions

In conclusion, dendrite formation and penetration through the GF separator have been identified as a major reason for the premature death of Na-O_2 batteries. Using a Nafion-Na^+ membrane as a part of composite separator to physically prevent dendrite penetration, significantly enhancement of the cyclability of Na-O_2 batteries was achieved. This allows us to identify the reaction between Na and electrolyte as another main contributor to the decline of performance. NMR, Raman and XPS were performed to prove that both Na triflate and DME solvent experience decomposition in the presence of Na and oxygen. Compared to the cathode, Na anode brought up more issues in Na-O_2 batteries. The findings emphasize the importance for improving the stability of Na anode and preventing oxygen crossover in Na-O_2 batteries.

Acknowledgements

This work was supported by Honda Research Institute, America, Inc.

Notes and references

[a] *Department of Chemistry and Biochemistry, The Ohio State University, 100 West 18th Avenue, Columbus, OH 43210, USA. Phone: (614) 247-7810. Fax: (614) 292-1685. Email: wu@chemistry.ohio-state.edu.*

[b] *Honda Research Institute, Inc., 1381 Kinnear Road, Columbus, OH 43212, USA.*

† Electronic Supplementary Information (ESI) available: Experimental details, Table S1-S4, Fig. S1-S6. See DOI: 10.1039/b000000x/

1 *(a)* G. Girishkumar, B. McCloskey, A. C. Luntz, S. Swanson and W. WilckeK, *J. Phys. Chem. Lett.*, 2010, **1**, 2193. *(b)* J. S. Lee, S. T. Kim, R. Cao, N. S. Choi, M. Liu, K. T. Lee and J. Cho, *Adv. Energy Mater.*, 2010, **1**, 34. *(c)* Y. Shao, F. Ding, J. Xiao, J. Zhang, W. Xu, S. Park, J. G. Zhang, Y. Wang and J. Liu, *Adv. Funct. Mater.*, 2013, **23**, 987.

2 *(a)* J. Lu, L. Li, J. B. Park, Y. K. Sun, F. Wu and K. Amine, *Chem. Rev.*, 2014, **114(11)**, 5611–5640. *(b)* P. G. Bruce, S. A. Freunberger, L. J. Hardwick and J. M. Tarascon, *Nat. Mater.*, 2012, **11**, 19. *(c)* F. Li, T. Zhang and H. Zhou, *Energy Environ. Sci.*, 2013, **6**, 1125.

3 P. Hartmann, C. L. Bender, M. Vracar, A. Garsuch, A. K. Durr, J. Janek and P. Adelhelm, *Nat. Mater.*, 2013, **12**, 228.

4 X. Ren and Y. Wu, *J. Am. Chem. Soc.*, 2013, **135**, 2923.

5 *(a)* S. A. Freunberger, Y. Chen, N. E. Drewett, L. J. Hardwick, F. Barde and P. G. Bruce, *Angew. Chem. Int. Ed.*, 2011, **50**, 8609. *(b)* Z. Peng, S. A. Freunberger, Y. Chen and P. G. Bruce, *Science*, 2012, **337(3)**, 563. *(c)* J. Lu, Y. Lei, K. C. Lau, X. Luo, P. Du, J. Wen, R. S. Assary, U. Das, D. J. Miller , J. W. Elam, H. M. Albishri, D A. El-Hady, Y. K. Sun, L. A. Curtiss and K. Amine, *Nature Communications*, 2013, **4**, 2383. *(d)* J. J. Xu, Z. L. Wang, D. Xu, L. L. Zhang and X. B. Zhang, *Nature Communications,* **4**, 2438.

6 *(a)* P. Hartmann, C. L. Bender, J. Sann, A.-K. Durr, M. Jansen, J. Janek and P. Adelhelm, *Phys. Chem. Chem. Phys.*, 2013, **15**, 11661-11672. *(b)* C. L. Bender, P. Hartmann, M. Vracar, P. Adelhelm and J. Janek, *Adv. Energy Mater.*, 2014, **4**, 1301863.

7 N. Zhao, C. Li, X. Guo, *Phys. Chem. Chem. Phys.*, 2014, **16(29)**, 15646.

8 B. D. McCloskey, J. M. Garcia and A. C. Luntz, *J. Phys. Chem. Lett.*, 2014, **5**, 1230.

9 *(a)* D. Kundu, E. Talaie, V. Duffort and L. F. Nazar, *Angew. Chem. Int. Ed.*, 2015, **54**, 2. *(b)* H. Pan, Y. S. Hu and L. Chen, *Energy Environ. Sci.*, 2013, **6**, 2338. (c) S. K. Das, S. Laub and L. A. Archer, *J. Mater. Chem. A*, 2014, **2**, 12623.

10 R. S. Assary, J. Lu, P. Du, X. Luo, X. Zhang, Y. Ren, L. A. Curtiss and K. Amine, *ChemSusChem*, 2013, **6**, 51.

11 X. Ren, K. C. Lau, M. Yu, X. Bi, E. Kreidler, L. A. Curtiss and Y. Wu, *ACS Appl. Mater. Interfaces*, 2014, **6(21)**, 19299.

12 *(a)* K. B. Hueso, M. Armand and T. Rojo, *Energy Environ. Sci.*, 2013, **6**, 734. *(b)* K. A. Mauritz and R. B. Moore, *Chem Rev*, 2004, **104**, 4535. *(c)* C. Heitner-Wirguin, *Journal of Membrane Science*, 1996, **120**, 33.

13 *(a)* K. Kreuer, A. Wohlfarth, C. C. Araujo, A. Fuchs and J. Maier, *ChemPhysChem*, 2011, **12**, 2558. *(b)* Y. Liu, L. Tan and L. Li, *Chem. Commun.*, 2012, **48**, 9858.

14 P. Hartmann, D. Grubl, H. Sommer, J. Janek, W. G. Bessler and P. Adelhelm, *J. Phys. Chem. C*, 2014, **118**, 1461.

15 *(a)* D. Aurbach, E. Zinigrad, Y. Cohen and H. Teller, *Solid State Ionics*, 2002, **148**, 405. *(b)* H. Kim, G. Jeong, Y. U. Kim, J. H. Kim, C. M. Park and H. J. Sohn, *Chem. Soc. Rev.*, 2013, **42**, 9011.

16 S. A. Freunberger, Y. Chen, Z. Peng, J. M. Griffin, L. J. Hardwick, F. Barde, P. Novak and P. G. Bruce, *J. Am. Chem. Soc.*, 2011, **133**, 8040.

17 E. Nasybulin, M. E. Gross, W. Xu, M. H. Engelhard and Ji-Guang Zhang, *J. Phys. Chem. C*, 2013, **117(6)**, 2635.

18 R. Younesi, M. Hahlin, M. Roberts and K. Edström, *Journal of Power Sources*, 2013, **225**, 40.

